Chinese Chemical Letters 36 (2025) 109621

Contents lists available at ScienceDirect

Chinese Chemical Letters

journal homepage: www.elsevier.com/locate/cclet

Bilayered Dion–Jacobson lead-iodine hybrid perovskite with aromatic spacer for broadband photodetection

Dongying Fu[a,b,*], Lin Pan[a], Yanli Ma[a], Yue Zhang[a]

[a] Institute of Crystalline Materials, Shanxi University, Taiyuan 030006, China
[b] State Key Laboratory of Quantum Optics and Quantum Optics Devices, Shanxi University, Taiyuan 030006, China

ARTICLE INFO

Article history:
Received 9 January 2024
Revised 30 January 2024
Accepted 7 February 2024
Available online 9 February 2024

Keywords:
Dion–Jacobson
Hybrid perovskite
Aromatic spacer
Two-dimensional
Broadband photodetection

ABSTRACT

Dion–Jacobson (DJ) phase hybrid perovskites have been proven to improve the photovoltaic performance of the devices due to its unique structure. At present, some DJ hybrid perovskites have been reported and used for photodetection filed, but most of them are based on lead-bromide systems, which is not conducive to construct broadband photodetection devices due to the limitation of intrinsic absorption. Herein, we constructed a bilayered DJ hybrid perovskite (3AMPY)(EA)Pb_2I_7 ($3AMPY^{2+}$ is 3-(aminomethyl)pyridinium, EA^+ is ethylammonium) using an aromatic spacer, which exhibit large current on/off ratios of ~10^4 under 520 and 637 nm illumination. In particular, the single crystal device based on (3AMPY)(EA)Pb_2I_7 shows a distinguished detectivity of 7.4×10^{12} Jones and a high responsivity of 0.89 A/W under 637 nm illumination. Such finding not only enriches the quantities of DJ hybrid perovskites, but also provides useful assistance for constructing high-performance optoelectronic device in the future.

Two-dimensional (2D) Dion–Jacobson (DJ) phase hybrid perovskites with diammonium spacers eliminate the van der Waals gap between adjacent inorganic layers, thus compensating for the disadvantage of Ruddlesden–Popper (RP) phase hybrid perovskites [1–18]. Compared with three-dimensional (3D) hybrid perovskites, the carrier transport performance of 2D hybrid perovskites in the out-of-plane direction is significantly limited due to the limitations of quantum wells and dielectric effects [19,20]. However, it is gratifying that DJ hybrid perovskites have superior out-of-plane carrier transport capabilities than RP hybrid perovskites. For example, Huang *et al.* directly observed fast carriers transport along out-of-plane direction in (4AMP)(MA)Pb_2I_7 (4AMP is 4-(aminomethyl)piperidinium, MA is methylammonium) [21]. This important feature is very beneficial for constructing high-performance optoelectronic devices. Due to the late start of research on DJ hybrid perovskite and the high difficulty in synthesis, the research on the structure–activity relationship of the optoelectronic devices constructed by them is far inferior to that of RP hybrid perovskites. According to the research reports, we know that the configuration of interlayer organic ammonium cations directly affects the structure and properties of hybrid perovskites [22–26]. Therefore, aromatic diammonium spacers have a higher dielectric constant than aliphatic diammonium spacers with the similar size, thereby increasing the degree of dielectric matching between the organic layer and inorganic layer, which is of particular concern in DJ hybrid perovskites [23,27–30]. In addition, due to the strong rigidity of aromatic diammonium, it is not easy to form 2D structure when constructing hybrid perovskites, resulting in a scarcity of kinds of DJ hybrid perovskites with aromatic spacers [31].

The absorption spectrum range and intensity reflect the responsiveness of hybrid perovskite to different wavelengths of light, and also affect the photodetection band range of such materials. Currently, most of the reported DJ hybrid perovskites photodetectors based on aromatic diammonium are lead-bromide systems, for example, (HIS)(DMA)Pb_2Br_7 (HIS^{2+} is histammonium and DMA^+ is dimethylammonium) [12], (2AMPY)$PbBr_4$ (2AMPY is 2-(aminomethyl)pyridinium) [24] and (3AMPY)(EA)Pb_2Br_7 (3AMPY is 3-(aminomethyl)pyridinium, EA is ethylammonium) [32]. Due to their absorption cutoff edge being mostly below 500 nm, the photodetection band range is relatively narrow. In order to broaden the light absorption range of DJ hybrid perovskites, it is urgent to design and construct more lead-iodine hybrid perovskites based on aromatic diammonium cations.

Herein, we have successfully constructed a 2D bilayered DJ hybrid perovskite (3AMPY)(EA)Pb_2I_7 using aromatic diammonium as spacer and EA as perovskitizer. Under the synergistic effect of $3AMPY^{2+}$ and EA^+ cations, (3AMPY)(EA)Pb_2I_7 shows a shorter interlayer spacing of 3.456 Å, which is superior to most lead-iodine

* Corresponding author at: Institute of Crystalline Materials, Shanxi University, Taiyuan 030006, China.
E-mail address: dyfu@sxu.edu.cn (D. Fu).

https://doi.org/10.1016/j.cclet.2024.109621
1001-8417/

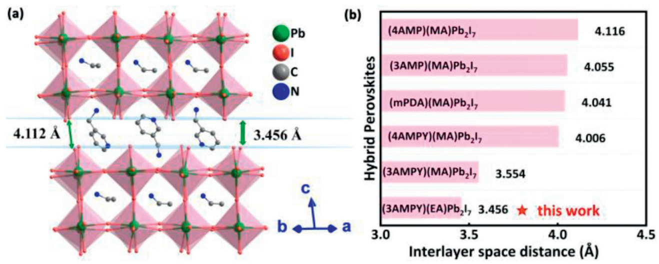

Fig. 1. (a) The structure of bilayered DJ hybrid perovskite (3AMPY)(EA)Pb_2I_7 at 200 K. (b) Comparison of the interlayer spacing between (3AMPY)(EA)Pb_2I_7 and other lead-iodine DJ hybrid perovskites.

DJ hybrid perovskites. Benefiting from the shorter interlayer spacing and wider light absorption range, single crystal devices based on (3AMPY)(EA)Pb_2I_7 exhibit excellent photo-response under 520 and 637 nm light irradiation, with a current on/off ratios of up to 10^4.

The single crystal of (3AMPY)(EA)Pb_2I_7 was synthesized by regulating the stoichiometric ratio of $Pb(CH_3COO)_2 \cdot 3H_2O$, EA, and 3AMPY in HI (55%–58%) solution. The single crystal structure of (3AMPY)(EA)Pb_2I_7 was shown in Fig. 1a, which contains double-layered $[Pb_2I_7]_n$ inorganic framework with the EA^+ cations enclosed in the perovskite cages. Unlike in RP hybrid perovskites, there is only monolayered organic $3AMPY^{2+}$ cations lying between the adjacent inorganic layer in (3AMPY)(EA)Pb_2I_7, which results in a shorter interlayer spacing of 3.456 Å. In addition, we also compared the interlayer spacing of other lead-iodine DJ hybrid perovskites constructed with aromatic diammonium (Fig. 1b and Table S1 in Supporting information), and the results showed that (3AMPY)(EA)Pb_2I_7 we constructed has the shortest interlayer spacing (Table S1). The shorter interlayer spacing reduces the difficulty of electron transfer in the out-of-plane direction, which is crucial for the performance of the devices. Moreover, the shorter interlayer spacing results in an I–I distance of only 4.112 Å, greatly increasing the interaction between adjacent inorganic sheets. The single-crystal X-ray diffraction (SCXRD) results indicate that (3AMPY)(EA)Pb_2I_7 belongs to the centrosymmetric space group of $P2_1/c$ with unit cell parameters of $a = 16.3167(7)$ Å, $b = 18.2945(7)$ Å, $c = 8.8253(4)$ Å and $\beta = 98.490(2)$ at 200 K. And the selected Pb–I bond lengths, Pb–I–Pb bond angels, I–Pb–I bond angles were provided in Tables S2–S4 (Supporting information). Moreover, the phase purity of (3AMPY)(EA)Pb_2I_7 has been verified by powder X-ray diffraction (PXRD) patterns in Fig. S1 (Supporting information). The thermal stability of (3AMPY)(EA)Pb_2I_7 was shown in Fig. S2 (Supporting information), there was no significant decomposition below 535 K, indicating its high thermal stability.

Next, we also analyzed the influence of perovskitizers on the structure in DJ hybrid perovskites. As shown in Fig. 2, compared with smaller size of MA (2.17 Å), the introduction of EA (2.74 Å) significantly leads to more distortion of the inorganic $[PbI_6]$ octahedra. For quantitative analysis, we introduced the octahedra asymmetry parameter Δd, which is calculated through the following formula [33]:

$$\Delta d = \left(\frac{1}{6}\right) \sum \left[\frac{d_n - d}{d}\right]^2 \qquad (1)$$

where d is the mean Pb–I bond length and d_n are the six individual Pb–I bond length in the octahedra. Through calculation, we found that the degree of distortion of the octahedron in (3AMPY)(EA)Pb_2I_7 (5.09×10^{-4}) is significantly greater than that in (3AMPY)(MA)Pb_2I_7 (1.73×10^{-4}) [4], indicating that the influence of perovskitizers on the structure is very obvious. This result is similar to the reported hybrid perovskites $(BA)_2(EA)_2Pb_3I_{10}$ and

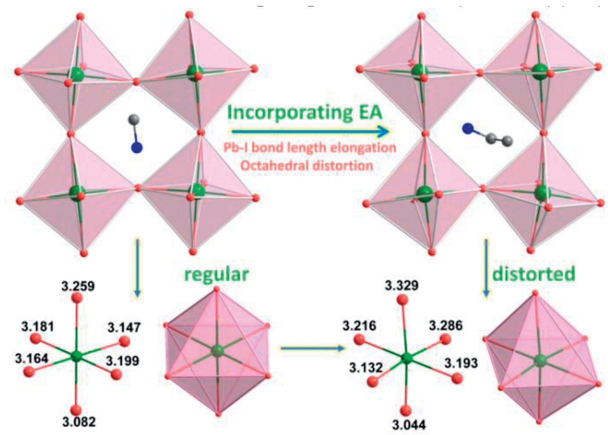

Fig. 2. The effect of different perovskitizers on the inorganic frameworks.

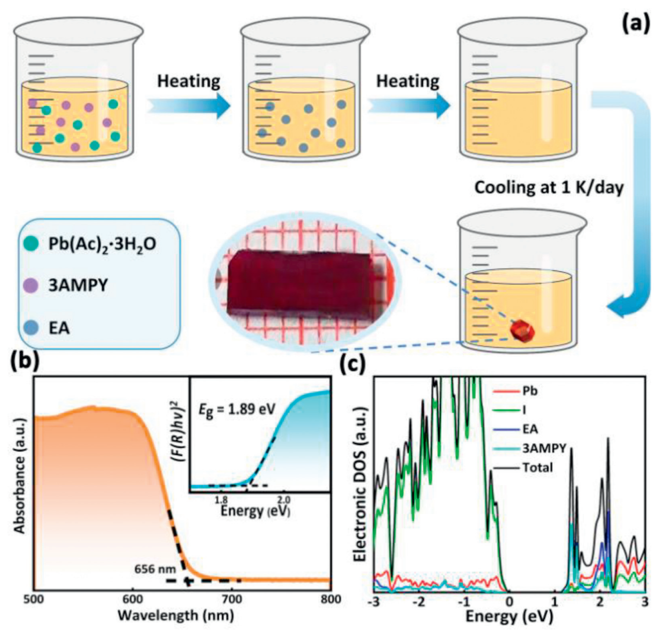

Fig. 3. (a) Process diagram for synthesizing (3AMPY)(EA)Pb_2I_7 bulk single crystal. (b) UV–vis absorption spectrum of (3AMPY)(EA)Pb_2I_7, inset is the band gap from *Tauc* equation. (c) The partial density of state (PDOS) spectra of (3AMPY)(EA)Pb_2I_7.

$(BA)_2(MA)_2Pb_3I_{10}$ (BA is *n*-butylammonium), which belong to the RP type hybrid perovskites [34]. The large octahedral distortion has a highly impact on the luminescent performance of materials, thus laying the foundation for the future use of such perovskites in the field of luminescence [34]. In addition, the introduction of large size of EA perovskitizer result in an average Pb-I bond length in (3AMPY)(EA)Pb_2I_7 (3.20 Å) greater than that in (3AMPY)(MA)Pb_2I_7 (3.164 Å). The Pb–I bond length also has a certain impact on the band gap of hybrid perovskites. Moreover, the distortion levels of $[PbI_6]$ octahedra can also be quantified by defining the distortion index (D) (bond length), quadratic elongation (λ) and bond angle variance (σ^2) based on Pb–I bond lengths and Pb–I–Pb bond angles through VESTA software [4]. The values of D, λ and σ^2 are listed in Table S5 (Supporting information). From these data, we can see that the distortion of $[PbI_6]$ octahedra in (3AMPY)(EA)Pb_2I_7 is more seriously than (3AMPY)(MA)Pb_2I_7.

For growing bulk single crystals of (3AMPY)(EA)Pb_2I_7, it is obtained by slow-cooling method in a saturated solution containing raw materials (Fig. 3a). Subsequently, we studied the optical absorption ability of (3AMPY)(EA)Pb_2I_7 in Fig. 3b. The

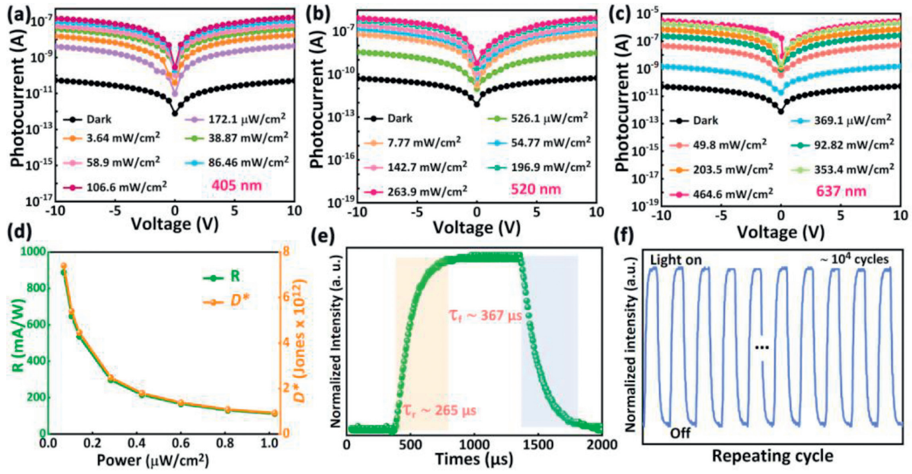

Fig. 4. Variation of photocurrent under different light power intensity and bias voltage, (a) 405 nm, (b) 520 nm, and (c) 637 nm. (d) Detectivity (D^*) and photoresponsivity (R) values with different incident light power density at 637 nm. (e) Rise and fall time of photocurrent responses at 637 nm. (f) The stability of the device based on $(3AMPY)(EA)Pb_2I_7$ after multi-cycling.

$(3AMPY)(EA)Pb_2I_7$ shows a sharp absorption edge at about 656 nm, affording the optical band gap (E_g) is ~1.89 eV according to the *Tauc* equation (Fig. 3b inset), which also can be seen it is a direct band gap characteristics. Due to the elongation of Pb–I bond lengths, the absorption cut off edge (λ_{cutoff}) of $(3AMPY)(EA)Pb_2I_7$ is obvious smaller than that of $(3AMPY)(MA)Pb_2I_7$ (705 nm) and $(3AMPY)(FA)Pb_2I_7$ (850 nm) [35], which fully demonstrates that the optical absorption range of the materials can also be controlled by changing the perovskitizers. In order to further investigate the semiconducting properties of $(3AMPY)(EA)Pb_2I_7$, we calculated its energy band structure using density functional theory (DFT) in Fig. S3 (Supporting information). Both the valence band maximum and conduction band minimum of $(3AMPY)(EA)Pb_2I_7$ are located at the Z point, once again confirmed its direct band gap semiconductor characteristics. Different from most reported hybrid perovskites whose semiconducting properties are mainly contributed by inorganic frameworks, in $(3AMPY)(EA)Pb_2I_7$, the interlayer aromatic diammonium $3AMPY^{2+}$ also contribute to the conduction band, which can be clearly observed in Fig. 3c. The semiconducting performance of $(3AMPY)(EA)Pb_2I_7$ has been verified from the above aspects, thus providing assurance for its use in photodetection.

Then, we assembled a single crystal device (Fig. S4 in Supporting information) based on $(3AMPY)(EA)Pb_2I_7$ and studied its photodetection performance at different wavelengths. The current–voltage (I–V) curves of $(3AMPY)(EA)Pb_2I_7$ were measured under 405 nm (Fig. 4a), 520 nm (Fig. 4b) and 637 nm (Fig. 4c) illumination. The $(3AMPY)(EA)Pb_2I_7$ device exhibits an ultralow dark current (I_{dark}) of 5.32×10^{-11} A at 10 V bias, which is comparable to other DJ hybrid perovskite, such as $(HIS)(DMA)Pb_2Br_7$ (1.97×10^{-11} A) [12]. The maximum photocurrent (I_{ph}) under 405 nm, 520 nm and 637 nm can reach to 1.45×10^{-7} A, 8.35×10^{-7} A, 2.91×10^{-6} A, respectively, corresponding to on/off ratios $((I_{ph}\text{-}I_{dark})/I_{dark})$ of up to $\sim10^3$ (405 nm) and $\sim10^4$ (520 nm and 637 nm) for the devices. This value exceeds the vast majority of hybrid perovskites optoelectronic devices, such as $(4\text{-}AMP)Cs_2Pb_3Br_{10}$ ($\sim10^3$) [36], $(2meptH_2)CsPb_2Br_7$ ($\sim10^3$) [37]. Photoresponsivity (R) and photodetectivity (D^*) are two important parameters for evaluating the performance of photodetectors. The value R is defined by equation $R = I_{ph}/(PS)$ [12], where the P is the incident light power density and S is the valid area of devices. The value D^* is estimated by the equation $D^* = I_{ph}/[PS(2qI_{dark})^{1/2}]$ [12], where q is the elementary electronic charge. The high crystal quality and low dark current make the devices based on $(3AMPY)(EA)Pb_2I_7$ single crystal exhibit excellent R (887.8 mA/W) and D^* (7.4×10^{12} Jones) under 637 nm laser irradiation. We can see that with the incident light power density increasing, the R and D^* value show a gradual decreasing variation in Fig. 4d. The D^* value of the $(3AMPY)(EA)Pb_2I_7$ single crystal device is comparable to commercial silicon photodetector with the D^* of 4×10^{12} Jones. The response time of the device includes rise time (τ_r) and decay time (τ_f) in Fig. 4e. The definition of response time for optoelectronic devices is that the time interval required for the photocurrent to increase from 10% of the peak to 90% (τ_r) and the time interval required for the photocurrent to decrease from 90% of its peak to 10% (τ_f). The τ_r and τ_f of the $(3AMPY)(EA)Pb_2I_7$ device are 265 μs and 367 μs, respectively. Finally, we tested the stability of the device under multiple cycles in Fig. 4f, the result shows that there was no obvious attenuation in the photocurrent of the device during the long time running. From structure to detection performance, it is sufficient to demonstrate that $(3AMPY)(EA)Pb_2I_7$ single crystal device have full potential in photodetection and are also an optional materials for constructing high-performance optoelectronic devices.

In summary, we constructed a bilayered DJ hybrid perovskite $(3AMPY)(EA)Pb_2I_7$ using aromatic diammonium as spacer and studied the photodetection performance of the single crystal devices. The introduction of EA as a larger perovskitizer into the system increases the stretching of the Pb–I bond length and the degree of distortion of the octahedron, confirming that different sizes of perovskitizer have a significant impact on the structure of hybrid perovskites. Moreover, the unique crystal structure of $(3AMPY)(EA)Pb_2I_7$ gives it a shorter interlayer spacing, and the single crystal device based on it show higher detectivity under 637 nm illumination. Our work not only enriches the kinds of muti-layer DJ hybrid perovskites, but also confirms that DJ hybrid perovskites constructed with aromatic diammonium have great potential as photodetection materials.

Declaration of competing interest

The authors declare no competing financial interest.

Acknowledgments

This work was financially supported by the National Natural Science Foundation of China (Nos. 22005183 and 22275117), the Program of State Key Laboratory of Quantum Optics and Quantum Optics Devices (No. KF202204).

References

[1] F. Zhang, S.Y. Park, C. Yao, et al., Science 375 (2022) 71–76.
[2] A. Dučinskas, G.Y. Kim, D. Moia, et al., ACS Energy Lett. 6 (2021) 337–344.
[3] C. Chen, X. Zhao, Y. Gong, et al., Chem. Mater. 35 (2023) 3265–3275.
[4] X. Li, W. Ke, B. Traoré, et al., J. Am. Chem. Soc. 141 (2019) 12880–12890.
[5] I.H. Park, K.C. Kwon, Z. Zhu, et al., J. Am. Chem. Soc. 142 (2020) 18592–18598.
[6] Y. Liu, H. Zhou, Y. Ni, et al., Joule 7 (2023) 1016–1032.
[7] W. Guo, Z. Yang, J. Dan, M. Wang, Nano Energy 86 (2021) 106129.
[8] L. Mao, P. Guo, M. Kepenekian, et al., J. Am. Chem. Soc. 142 (2020) 8342–8351.
[9] W. He, Y. Yang, C. Li, et al., J. Am. Chem. Soc. 145 (2023) 14044–14051.
[10] M. Guan, Y. Xie, Y. Zhang, et al., Adv. Mater. 35 (2023) 2210611.
[11] J. Chen, Z. Zhai, Q. Liu, H. Zhou, Nanoscale Horiz. 8 (2023) 1628–1651.
[12] Q. Fan, Y. Ma, H. Xu, et al., Adv. Opt. Mater. 11 (2023) 2202277.
[13] Y. Li, J.V. Milić, A. Ummadisingu, et al., Nano Lett. 19 (2019) 150–157.
[14] R. Shi, Z. Zhang, W.H. Fang, R. Long, J. Mater. Chem. A 8 (2020) 9168–9176.
[15] Y. Fan, Q. Chen, Z. Li, et al., Small 19 (2023) 2303814.
[16] H. Ye, Y. Peng, X. Shang, et al., Adv. Funct. Mater. 32 (2022) 2200223.
[17] K. Song, P. Zhou, L. Zong, et al., Chin. Chem. Lett. 34 (2023) 107464.
[18] Z. Wei, Y. Zhao, J. Jiang, et al., Chin. Chem. Lett. 31 (2020) 3055–3064.
[19] S. Yu, M. Abdellah, T. Pullerits, K. Zheng, Z. Liang, Adv. Funct. Mater. 31 (2021) 2104342.
[20] X. Zhang, T. Yang, X. Ren, Adv. Energy Mater. 11 (2021) 2002733.
[21] Z. Shi, Z. Ni, J. Huang, ACS Energy Lett. 7 (2022) 984–987.
[22] R. Zhao, R.P. Sabatini, T. Zhu, et al., J. Am. Chem. Soc. 143 (2021) 19901–19908.
[23] A. Dučinskas, G.C. Fish, M.A. Hope, et al., J. Phys. Chem. Lett. 12 (2021) 10325–10332.
[24] D. Fu, S. Wu, W. Cao, Z. Chen, X.M. Zhang, J. Mater. Chem. C 10 (2022) 9613–9620.
[25] L. Mao, W. Ke, L. Pedesseau, et al., J. Am. Chem. Soc. 140 (2018) 3775–3783.
[26] S.A. Cuthriell, C.D. Malliakas, M.G. Kanatzidis, R.D. Schaller, J. Am. Chem. Soc. 145 (2023) 11710–11716.
[27] D. Lu, G. Lv, Z. Xu, et al., J. Am. Chem. Soc. 142 (2020) 11114–11122.
[28] A. Ummadisingu, A. Mishra, D.J. Kubicki, et al., Small 18 (2022) 2104287.
[29] L. Gao, X. Li, B. Traoré, et al., J. Am. Chem. Soc. 143 (2021) 12063–12073.
[30] Z. Fang, X. Hou, Y. Zheng, et al., Adv. Funct. Mater. 31 (2021) 2102330.
[31] P.S. Klee, Y. Hirano, D.B. Cordes, A.M.Z. Slawin, J.L. Payne, Cryst. Growth Des. 22 (2022) 3815–3823.
[32] D. Fu, W. Jia, S. Wu, et al., Chem. Mater. 35 (2023) 2541–2548.
[33] L. Mao, Y. Wu, C.C. Stoumpos, M.R. Wasielewski, M.G. Kanatzidis, J. Am. Chem. Soc. 139 (2017) 5210–5215.
[34] Y. Fu, X. Jiang, X. Li, et al., J. Am. Chem. Soc. 142 (2020) 4008–4021.
[35] D. Fu, Z. Hou, Y. He, et al., ACS Appl. Mater. Interfaces 14 (2022) 11690–11698.
[36] Z. Wang, X. Zhang, H. Ye, T. Zhu, J. Luo, Chem. Eur. J. 28 (2022) e202200849.
[37] D. Fu, S. Wu, J. Xin, et al., Chem. Commun. 56 (2020) 14381–14384.